

PAPER

60-GHz third-order on-chip bandpass filter using GaAs pHEMT technology

To cite this article: Kai-Da Xu *et al* 2022 *Semicond. Sci. Technol.* **37** 055004

View the [article online](#) for updates and enhancements.

You may also like

- [Fiber-coupled superconducting nanowire single-photon detectors integrated with a bandpass filter on the fiber end-face](#)
W J Zhang, X Y Yang, H Li et al.
- [Extracting impedance changes from a frequency multiplexed signal during neural activity in sciatic nerve of rat: preliminary study *in vitro*](#)
J Hope, K Aristovich, C A R Chapman et al.
- [Small-signal modeling and parameter extraction method for a multigate GaAs pHEMT switch](#)
Lin Luo, Jun Liu, Guofang Wang et al.

ECS Toyota Young Investigator Fellowship



For young professionals and scholars pursuing research in batteries, fuel cells and hydrogen, and future sustainable technologies.


At least one \$50,000 fellowship is available annually.
More than \$1.4 million awarded since 2015!



Application deadline: January 31, 2023

Learn more. Apply today!

60-GHz third-order on-chip bandpass filter using GaAs pHEMT technology

Kai-Da Xu¹ , Xiaoyu Weng¹, Jianxing Li^{1,*}, Ying-Jiang Guo^{2,*}, Rui Wu³, Jianlei Cui⁴ and Qiang Chen⁵

¹ School of Information and Communications Engineering, Xi'an Jiaotong University, Xi'an 710049, People's Republic of China

² Microsystem and Terahertz Research Center in China Academy of Engineering Physics, Chengdu 610200, People's Republic of China

³ National Key Laboratory of Microwave Imaging Technology, Aerospace Information Research Institute, Chinese Academy of Sciences, Beijing 100094, People's Republic of China

⁴ State Key Laboratory for Manufacturing Systems Engineering, Xi'an Jiaotong University, Xi'an 710049, People's Republic of China

⁵ Department of Communications Engineering, Tohoku University, Sendai 980-8579, Japan

E-mail: jianxingli.china@xjtu.edu.cn and guoyingjiang1@gmail.com

Received 1 January 2022, revised 4 March 2022

Accepted for publication 9 March 2022

Published 29 March 2022



Abstract

A 60 GHz third-order on-chip bandpass filter (BPF) based on half-mode substrate integrated waveguide (HMSIW) cavity is synthesized using GaAs pHEMT technology. Two coupling slots are etched to divide the HMSIW cavity into three resonators, and then a third-order Chebyshev BPF is designed with predicted transmission zero, return loss and bandwidth through the synthesis method. The theoretical and extracted external quality factor and coupling coefficients are used to determine the dimensions of the BPF. For demonstration, a BPF sample with a bandwidth of 29.2% is fabricated, and its simulations and measurements are in good agreement.

Keywords: bandpass filter, GaAs technology, millimeter wave circuits, on-chip devices

(Some figures may appear in colour only in the online journal)

1. Introduction

With the fast development of the fifth-generation (5G) and next-generation communications, designing millimeter-wave high-integration on-chip bandpass filters (BPFs) has been of great interest recently. Several semiconductor technologies are applied for the design of the BPFs, such as flexible polyimide substrate [1], compound column III–V [2–8], and SiGe/C-MOS [9–16]. Especially, the design of 60 GHz on-chip BPFs has been a hot research topic since this frequency band is a promising solution to future Gb/s wireless communication.

In [8], an E-shaped dual-mode resonator and a stepped impedance resonator are used to construct a two-pole BPF at 60 GHz, whose design method is inspired from the filter topology fabricated on the printed circuit boards. In [9], a square

ring one-wavelength resonator with a perturbation patch is employed to design a 60 GHz dual-mode BPF, and this method is often adopted for the filter design at low frequency, where the characteristics and size of the BPF are hardly improved. In [10] and [12], two second-order BPFs working at 60 GHz are presented using CMOS technology, but it is difficult to extend the design of higher order BPFs with low loss.

The GaAs pHEMT-based technology has been widely applied in communication circuits and systems. So far, few work on the synthesis of the millimeter-wave on-chip BPFs using GaAs technology has been presented. In this paper, using a half-mode substrate integrated waveguide (HMSIW) cavity, a third-order GaAs-based BPF working at 60 GHz is synthesized and fabricated. The measured results show that the proposed BPF has wide bandwidth and high frequency selectivity, which are in good agreement with the simulated ones. It validates the correctness of the synthesis method for the on-chip BPF.

* Authors to whom any correspondence should be addressed.

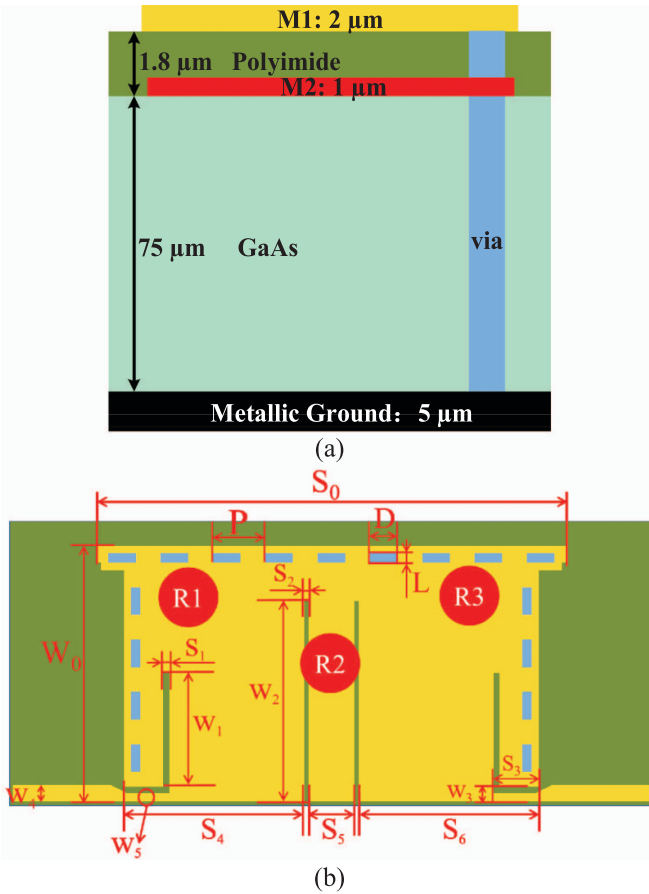


Figure 1. (a) Stack-up of the employed 0.15 μm GaAs pHEMT technology. (b) Layout of the proposed BPF.

2. Synthesis of 60 GHz third-order on-chip BPF

Figure 1 shows the proposed on-chip BPF based on HMSIW cavity using 0.15 μm GaAs pHEMT technology, where the relative permittivities of the GaAs and polyimide films are 12.9 and 2.9, respectively. The symmetrical structure of this filter consists of two microstrip feed lines and one HMSIW cavity with four slots etched on the top metal layer (i.e. M1 layer). The M2 layer as seen in figure 1(a) is not used in this work. Two slots in the middle as the coupling slots can be seen as capacitors, which provide the electric coupling between the adjacent resonators. Therefore, the HMSIW cavity is divided into three resonators, namely, Resonator 1 (R_1), Resonator 2 (R_2) and Resonator 3 (R_3). It should be noted that R_1 and R_3 are quarter-mode SIW resonators, whereas R_2 is a quarter-wavelength microstrip resonator. Besides, another two slots near the feeding as matching slots are used to achieve the desired impedance matching between the feed lines and the HMSIW cavity. As shown in the layout of the proposed filter, the transversal length of R_2 (S_5) is shorter than R_1 and R_3 , which is different from the BPF with same dimensions of resonators in [17]. Therefore, the cross coupling between non-adjacent resonators should be taken into consideration, which will introduce a transmission zero (TZ) to the response of this proposed BPF.

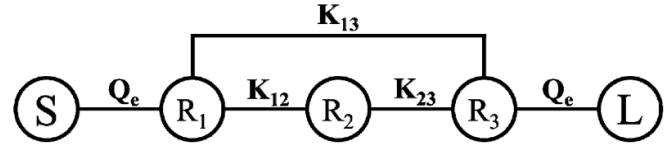


Figure 2. Coupling scheme of the proposed structure, where S and L represent source and load ports, respectively.

The coupling scheme of the proposed structure is shown in figure 2, where Q_e is the external quality factor and K_{ij} ($i, j = 1, 2, 3, i \neq j$) is the coupling coefficient. The K_{12} and K_{23} represent the coupling coefficients between two adjacent resonators while K_{13} is the coupling coefficient between two non-adjacent resonators R_1 and R_3 . According to the coupling mechanism, the frequency response of the BPF can be determined by the values of the external quality factor and the coupling coefficients.

Generally, the values of Q_e and K_{ij} can be derived through the synthesis method of filters [18]. If the third-order Chebyshev filter ($N = 3$) is designed to have the predicted TZ at the angular frequency of +1.7 and return loss of 15 dB in pass-band, the $(N + 2)$ coupling matrix \mathbf{M}_1 can be synthesized and expressed as follow:

$$\mathbf{M}_1 = \begin{bmatrix} 0 & -0.5732 & -0.3448 & 0.6689 & 0 \\ -0.5732 & 1.2593 & 0 & 0 & 0.5732 \\ -0.3448 & 0 & -1.1881 & 0 & 0.3448 \\ 0.6689 & 0 & 0 & -0.3965 & 0.6689 \\ 0 & 0.5732 & 0.3448 & 0.6689 & 0 \end{bmatrix}. \quad (1)$$

It is obvious that the matrix (1) has the transversal coupling structure, which is not suitable for the proposed BPF. However, \mathbf{M}_1 can be transformed to the folded form by similarity transforms [18]. Consequently, the coupling matrix of the folded network is transferred as:

$$\mathbf{M}_2 = \begin{bmatrix} 0 & -0.9460 & 0 & 0 & 0 \\ -0.9460 & 0.1062 & -0.7644 & 0.5028 & 0 \\ 0 & -0.7644 & -0.5377 & -0.7644 & 0 \\ 0 & 0.5028 & -0.7644 & -0.1062 & 0.9460 \\ 0 & 0 & 0 & 0.9460 & 0 \end{bmatrix}. \quad (2)$$

The Q_e and K_{ij} can be calculated from the entries of \mathbf{M}_2 by [19]:

$$Q_e = \frac{1}{m_{S1}^2 \cdot FBW}, \quad K_{ij} = m_{ij} \cdot FBW, \quad (3)$$

where FBW is the fractional bandwidth of BPF. Here, the center frequency of 60 GHz and the FBW of 30% are as the design specifications of BPF. Accordingly, the theoretical Q_e and K_{ij} are calculated as:

$$Q_e = \frac{1}{0.9460^2 \times 0.3} = 3.7247 \quad (4a)$$

$$K_{12} = K_{23} = |-0.7644 \times 0.3| = 0.2293 \quad (4b)$$

$$K_{13} = |0.5028 \times 0.3| = 0.1508. \quad (4c)$$

The calculation results of coupling coefficients in (4b) and (4c) are the absolute values, because only the magnitudes of coupling coefficients are needed to determine the physical dimensions of the coupling slots [18].

To obtain the proper dimensions, the actual values of external quality factor and coupling coefficients are extracted using the full-wave electromagnetic simulation software Ansys HFSS. Firstly, the dimensions of the HMSIW cavity is adjusted to get its resonance frequency of 60 GHz. Then, according to the coupling mechanism, the cross coupling between R₁ and R₃ (i.e. K₁₃) is of great importance on the generation of TZ. The location of the TZ will be changed against the value of K₁₃. However, it is difficult to accurately extract K₁₃ through simulation to fit well with the theoretical value of K₁₃. This is due to the fact that the resonator R₂ is placed along the coupling path of R₁ and R₃, resulting in K₁₃ dependent on the dimensions of the resonator R₂ mainly. Therefore, we should simulate different values of S₅ to meet the theoretical value of K₁₃. And the dimensions of R₁ and R₃ can be calculated based the size of HMSIW cavity and R₂. After that, the external quality factor and coupling coefficients could be extracted easily.

According to the theory of coupled resonators, the external quality factor can be numerically extracted by simulating an individually loaded resonator based on driven-mode through the following equation [19]:

$$Q_e = \frac{f_0}{\Delta f_{\pm 90^\circ}}, \quad (5)$$

where f_0 denotes the resonance frequency at the excitation port of the first resonator (i.e. R₁ or R₃) in the HMSIW cavity, and $\Delta f_{\pm 90^\circ}$ is determined from the frequency at which the phase $\pm 90^\circ$ with respect to the absolute phase at f_0 . Figure 3 depicts that the extracted Q_e is dependent on the slot width S_1 and the slot length W_1 . As W_1 increases, the external quality factors for different values of S_1 will all decrease. For the same slot length W_1 , the Q_e will be gradually reduced as S_1 increases.

Furthermore, the coupling coefficients can also be extracted through the eigenmode simulation of the two coupled resonators using the following formula [19]:

$$K_{12} = K_{23} = \pm \frac{1}{2} \left(\frac{f_{01}}{f_{02}} + \frac{f_{02}}{f_{01}} \right) \sqrt{\left(\frac{f_{p2}^2 - f_{p1}^2}{f_{p2}^2 + f_{p1}^2} \right)^2 - \left(\frac{f_{02}^2 - f_{01}^2}{f_{02}^2 + f_{01}^2} \right)^2}, \quad (6)$$

where f_{01} and f_{02} denote the self-resonant frequencies of R₁ and R₂, respectively, f_{p1} and f_{p2} represent the two resonance frequencies of the coupled resonators. All the resonance

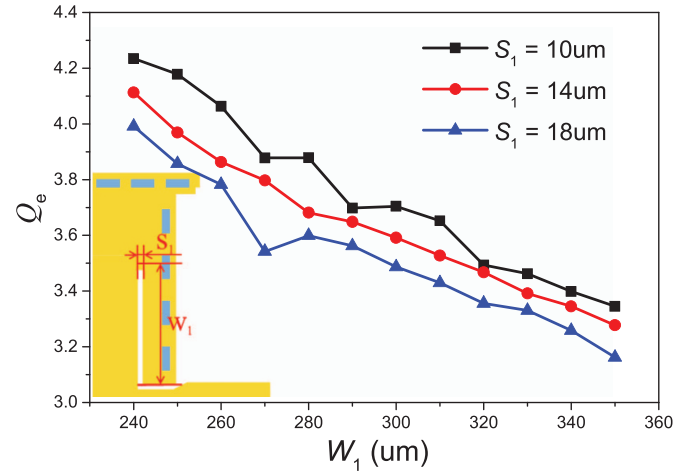


Figure 3. Extracted external quality factor Q_e versus S_1 and W_1 .

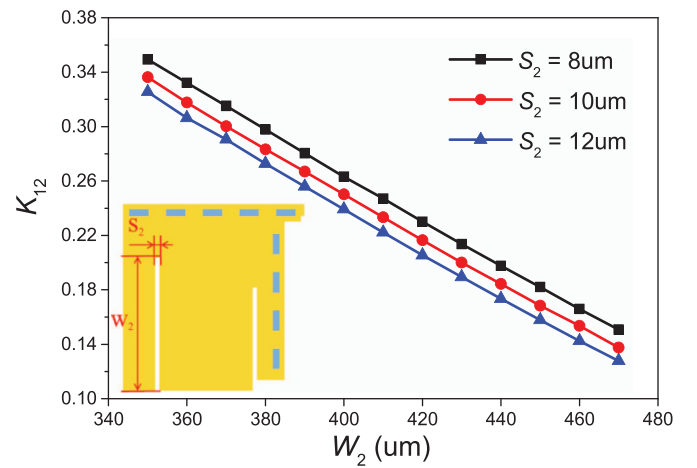


Figure 4. Extracted coupling coefficient K_{12} versus S_2 and W_2 .

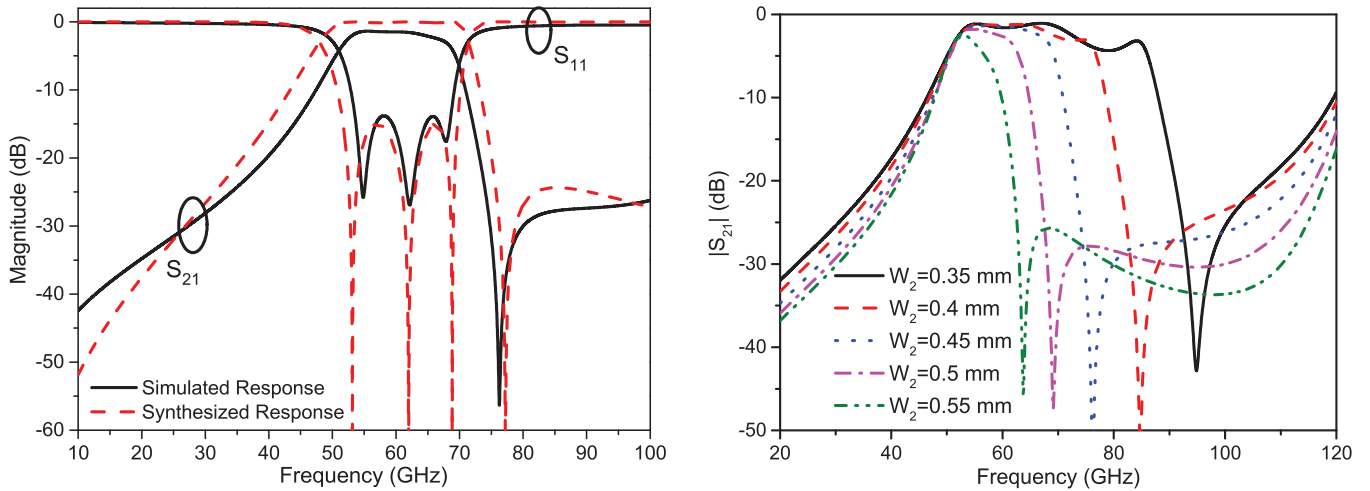
frequencies can be obtained through eigenmode simulations. The extracted results of coupling coefficients versus S_2 and W_2 are plotted in figure 4. It can be found that the larger the dimensions of the coupling slots are, the weaker the coupling between R₁ and R₂ will be.

Based on the theoretical values of Q_e , K_{12} and K_{23} calculated in (4), the initial dimensions of the BPF are selected according to these extracted curves in figures 3 and 4. Then, the designed BPF is fine-tuned through the full-wave electromagnetic (EM) simulation software Ansys HFSS to compensate the influence from parasitic parameters. The final dimensions are tabulated in table 1.

The synthesized frequency response derived from (2) and full-wave EM simulated response are both plotted in figure 5. The transmission poles and TZ of simulated results almost appeared in the same positions with those of synthesized results. Regardless of the loss influence, the simulated and synthesized S-parameters agree reasonably with each other, which verifies the correction of the synthesis process and the extraction of parameters.

Table 1. Dimensions of the proposed BPF.

Parameter	Value (μm)	Parameter	Value (μm)	Parameter	Value (μm)
W_0	561	S_0	1035	S_6	396
W_1	286	S_1	14	P	115
W_2	450	S_2	10	D	60
W_3	32	S_3	100	L	20
W_4	35	S_4	396		
W_5	18	S_5	100		

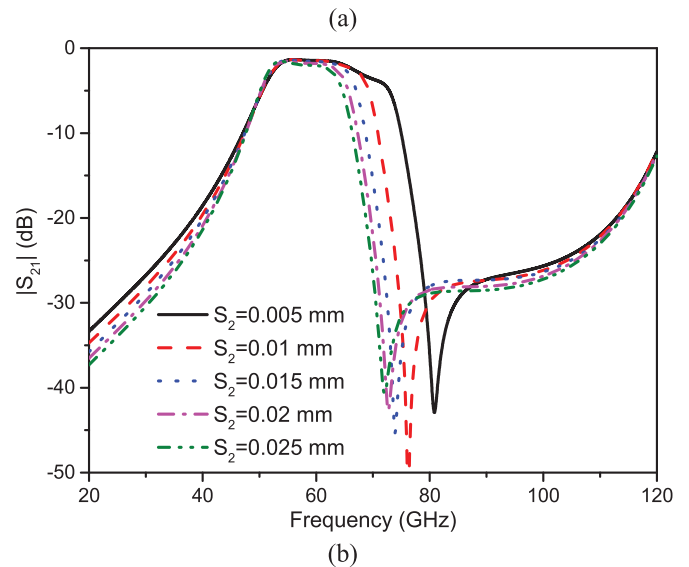
**Figure 5.** Comparison of the synthesized response and the simulated response.

According coupled resonator theory, we can change the cross coupling and the main coupling to control the position of TZ. The cross coupling between R_1 and R_3 is mainly related with the dimensions of the resonator R_2 . However, the change of R_2 will not only control the cross coupling, but also influence the main coupling between adjacent resonators. Therefore, we can choose the coupling slot as the key parameter to adjust the position of TZ, which is shown in figure 6. With the increase of W_2 and S_2 , the coupling coefficient is decreased and the position of TZ shifts to lower frequency.

3. Implementation and measurements

For further demonstration of the proposed HMSIW BPF, the above mentioned example is fabricated and then measured via an on-wafer ground-signal-ground probing using a vector network analyzer. The measurement setup and die photograph of the proposed BPF are shown in figure 7.

The simulated and measured S_{11} and S_{21} of the BPF are shown in figure 8, which agree well with each other. The measured results show that the presented BPF has a center frequency at 60.2 GHz with a 3 dB bandwidth from 51.4 to 69 GHz (i.e. 29.2%). The measured insertion losses are at the range between 1.99 and 2.72 dB within the passband, and the return losses are better than 13.9 dB. These results

**Figure 6.** The position of TZ with different dimensions of coupling slots. (a) $S_2 = 0.1$ mm, (b) $W_2 = 0.45$ mm.

are basically coincident with the design specifications of BPF mentioned in section 2. The die photograph of the filter can be seen in the inset of figure 7. The chip size, excluding the feedings, is 1.035 mm \times 0.561 mm. The performance comparisons between the proposed BPF and some reported works are tabulated in table 2.

The reference in the table means the reference, and FBW is the fractional bandwidth.

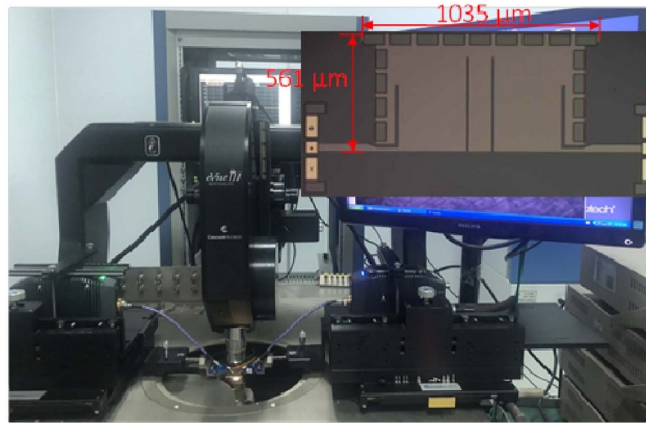


Figure 7. Measurement setup and die photograph of the proposed BPF.

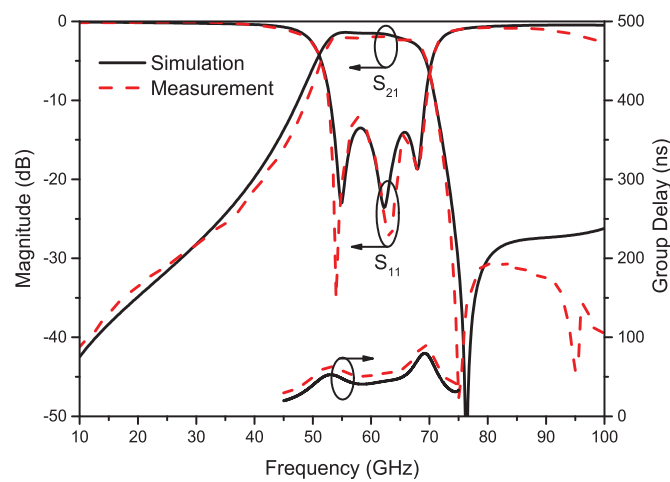


Figure 8. Simulated and measured S-parameters and group delays of the proposed BPF.

Table 2. Performance comparisons with some reported BPFs.

Reference	f_0 (GHz)	3 dB FBW (%)	Insertion loss	Order of BPF	Circuit size (mm × mm)	Technology
[5]	93	3.4	4.3	3	4.2×2.2	ICP GaAs
[8]	60	24.7	1.2	2	0.58×0.4	IPD GaAs
[9]	64	18.8	4.9	2	0.71×0.71	$0.18 \mu\text{m}$ CMOS
[12]	26.5	50.9	3.8	1	0.39×0.45	$0.13 \mu\text{m}$ SiGe
[14]	18	66.7	2.9	2	0.318×0.392	$0.13 \mu\text{m}$ SiGe
This work	60	29.2	1.99	3	1.035×0.561	$0.15 \mu\text{m}$ GaAs

4. Conclusion

A 60 GHz on-chip BPF based on HMSIW cavity is proposed with a TZ at the upper stopband. Through the synthesis method, the theoretical values of external quality factor and coupling coefficients are calculated from a third-order Chebyshev BPF prototype, and then the dimensions of BPF are determined. The presented 60 GHz BPF has a broad bandwidth, low insertion loss and sharp roll-off skirt at the right edge of the passband, which can be readily applied in modern or even next-generation communication systems.

Data availability statement

The data that support the findings of this study are available upon reasonable request from the authors.

Acknowledgments

National Key Research and Development Program of China (2019YFB1803205); NSAF Joint Fund (U2130102); Natural Science Foundation of Shaanxi Province (2021JQ-060); State Key Laboratory of Advanced Optical Communication

Systems Networks (2022GZKF020); Fundamental Research Funds for the Central Universities (xzd012020058); ‘Siyuan Scholar’ Fellowship of XJTU.

ORCID iD

Kai-Da Xu  <https://orcid.org/0000-0001-9408-1347>

References

- [1] Gong J, Wang Z, Qu H and Cang D 2021 *Semicond. Sci. Technol.* **36** 125008
- [2] Kaletta U C *et al* 2013 *Semicond. Sci. Technol.* **28** 065013
- [3] Xu K D, Xia S, Jiang Y, Guo Y, Liu Y, Wu R, Cui J and Chen Q 2022 *IEEE J. Electron Devices Soc.* **10** 152–6
- [4] Xu K, Guo Y, Liu Y, Deng X, Chen Q and Ma Z 2021 *IEEE Electron Device Lett.* **42** 1120–3
- [5] Xiao Y *et al* 2019 *IEEE Microw. Wirel. Compon. Lett.* **29** 104–6
- [6] Guo Y *et al* 2020 *IEEE Electron Device Lett.* **41** 1165–8
- [7] Xu K *et al* 2021 *IEEE Photonics Technol. Lett.* **33** 255–8
- [8] Li L *et al* 2018 *IEEE Electron Device Lett.* **39** 12–14
- [9] Hsu C *et al* 2008 *IEEE Electron Device Lett.* **29** 246–8
- [10] Franc A *et al* 2012 *IEEE Trans. Electron Devices* **59** 1219–26
- [11] Saadi A *et al* 2018 *AEU Int. J. Electron. Commun.* **84** 1–7
- [12] Abd El-Hameed A *et al* 2017 *IEEE Microw. Wirel. Compon. Lett.* **27** 818–20
- [13] Mahmoud N *et al* 2016 *IEEE Microw. Wirel. Compon. Lett.* **26** 681–3
- [14] Li M *et al* 2018 *IEEE Trans. Electron Devices* **65** 5453–9
- [15] Zhu H *et al* 2018 *IEEE Trans. Circuits Syst. I* **65** 4061–71
- [16] Xu K *et al* 2020 *IEEE Electron Device Lett.* **41** 1617–20
- [17] Wang Y *et al* 2007 *IEEE Microw. Wirel. Compon. Lett.* **17** 265–7
- [18] Cameron R *et al* 2018 *Microwave Filters for Communication Systems: Fundamentals, Design and Applications* 2nd edn (Hoboken, NJ: Wiley)
- [19] Hong J *et al* 2005 *Microstrip Filters for RF/Microwave Applications* 2nd edn (Hoboken, NJ: Wiley)